Appl Phys A (2008) 93: 293–301
DOI 10.1007/s00339-008-4824-4

Applied Physics A
Materials Science & Processing

In-situ formation and detailed analysis of imine bonds for the construction of conjugated aromatic monolayers on Au(111)

Y. Luo · M. Piantek · J. Miguel · M. Bernien · W. Kuch · R. Haag

Received: 21 January 2008 / Accepted: 9 July 2008 / Published online: 23 August 2008

Abstract We present the synthesis of 4′-amino-4-mercaptobiphenyl (AMB) and its deposition from solution onto Au(111) substrates. The resulting organic thin films were characterized by contact angle, infrared reflection absorption spectroscopy (IRRAS), X-ray photoelectron spectroscopy (XPS), and near edge X-ray absorption fine structure (NEXAFS) measurements. It is demonstrated that the majority of AMB molecules are coupled to the gold surface via S–Au covalent bonds, although only little orientational order of the AMB layer could be detected by NEXAFS. Furthermore, aromatic imine bonds between AMB and 4-hydroxybenzaldehyde (HB), 4-carboxybenzaldehyde (CB), 4-methylbenzaldehyde (MB), or 4-(trifluoromethyl) benzaldehyde (TMB) have been successfully formed. As a result of the limited order, this coupling reaction was incomplete. Nevertheless, the experimental results confirmed the formation of conjugated aromatic imine bonds.

PACS 82.35.Np · 81.16.Fg · 87.64.km · 87.64.kd

1 Introduction

Self-assembled monolayers (SAMs) are well ordered and densely packed monomolecular organic films which are spontaneously grown from solution or from the gas phase by adsorption of reactive molecules with an affinity of their headgroup to a substrate, resulting in chemical bond formations [1, 2]. The terminating functional groups of the SAMs define the properties of the surface, like wetting [3, 4], corrosion [5], biocompatibility [6, 7], and electron transport [8].

In the past, SAMs of alkanethiolates on gold were extensively and thoroughly studied, whereas thiophenolate SAMs are still relatively unexplored. Compared to the alkanethiolate SAMs, the latter system has several advantages: First, it is more stable because phenyl thiolates are planar molecules and more rigid than alkane chains [9]. Second, the replacement of substituting groups of phenyl thiolate is relatively easy, thus altering the nature of the SAMs [10]. Wöll et al. [11–13], Ulman et al. [10, 14–16], and Zharnikov et al. [17, 18] pioneered this field, namely the preparation and the spectroscopic characterization of oligophenyl and nonsubstituted and substituted biphenylthiolates (-CH_3, -OH, -CF_3, -CH_2SH, -SH, -NO_2, -$N(CH_3)_2$, and halogen) SAMs. They concluded that a longer phenyl backbone introduces a greater interchain interaction and results in a more upright orientation. Moreover, an insertion of a methylene unit between the phenyl ring and the thiol head group improved the order of formed monolayers [11]. Free amino groups (NH_2) as the substituent on the ω-position have only been reported once for a theoretical study on the energetics at the interface between a metal substrate and molecular monolayers [19].

Here we will introduce the monolayer preparation of 4′-amino-4-mercaptobiphenyl (AMB) on Au(111) and the in-situ formation of aromatic imine bonds (Fig. 1). It is well known that an imine can be synthesized by the nucleophilic addition of amine to ketone or aldehyde giving a hemiaminal -C(OH)(NHR)-, followed by the elimination of water to yield the imine [20]. Although it is an efficient reaction widely used in organic synthesis, its

Y. Luo · R. Haag (✉)
Institut für Chemie und Biochemie, Freie Universität Berlin, Takustr. 3, 14195 Berlin, Germany
e-mail: haag@chemie.fu-berlin.de
Fax: +49-30-83853357

M. Piantek · J. Miguel · M. Bernien · W. Kuch
Institut für Experimentalphysik, Freie Universität Berlin, Arnimallee 14, 14195 Berlin, Germany

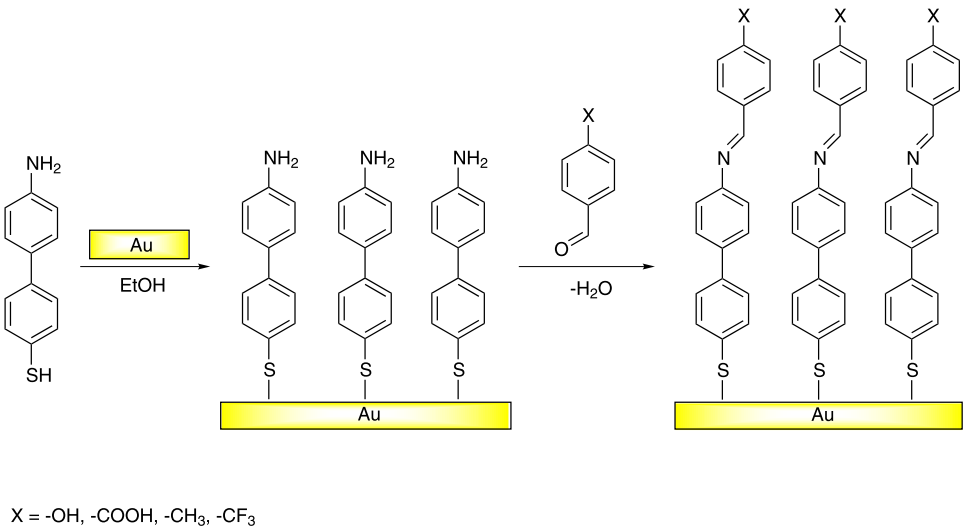

Fig. 1 The idealized conjugated SAMs on Au(111) fabricated by in-situ imine formation

formation on gold surfaces has not been fully investigated. Rosink et al. [21] investigated the self-assembly of π-conjugated azomethine oligomers by sequential deposition of monomers from solution. The oligomer chain growth was achieved by alternating condensations between 1,4-diaminobenzene and 1,4-benzdialdehyde. They used scanning tunneling microscopy, ellipsometry, and X-ray photoelectron spectroscopy (XPS) to analyze all the fabrication steps. However, no direct evidence for the imine formation was obtained. More recently, Klare et al. [22] constructed upright monolayers of cruciform π-systems on a gold surface with the same chemical reaction. From the analysis of infrared reflection absorption spectroscopy (IRRAS), they found that the ν(C=O) stretch of the aldehyde at 1710 cm^{-1} disappeared after the condensation reaction. However, the imine bond formation could not be proven because the imine stretch overlaps with the oxazole stretch.

To avoid these potential shortcomings, we have selected AMB as a template for in-situ formation of aromatic imine bonds on Au(111). In the following, we will introduce the preparation of SAMs from different solutions and provide a detailed analysis based on contact-angle, IRRAS, XPS, and NEXAFS (near edge X-ray absorption fine structure) measurements.

2 Experimental

2.1 Materials

Commercial reagents were purchased from Acros or Merck with ACS grade and were used without further purification. All solvents were obtained from Acros or Merck. Gold-coated glass and gold-coated mica wafers were purchased from Arrandee and Georg Albert Physical Vapor Deposition, respectively.

2.2 Synthesis of 4′-amino-4-mercaptobiphenyl

Generally, aromatic thiol compounds are synthesized by deprotecting their protection groups, like acetyl [23] and methyl [24], since these compounds are usually easily oxidized and reactive under basic conditions. In our study, we synthesized the AMB via direct chlorosulfonation followed by reduction (Fig. 2).

4-Nitrobiphenyl (Step 1 in Fig. 2) was obtained in high yield by the Suzuki coupling reaction (Appendix 1) [25]. Either flash chromatography or crystallization can be used for effective purification. Chlorosulfonation [26, 27] was managed in two steps in order to decrease the amount of used chlorosulfonic acid (Appendices 2–3), and no further purification was necessary before reduction to disulfide (Appendix 4). Finally, the disulfide and nitro functional groups were reduced at the same time by iron and hydrochloric acid (Appendix 5) [28]. The yield of crude product with a purity of 90%, estimated from nuclear magnetic resonance (NMR) spectra, can be as high as 94%. However, after the purification by column chromatography, the yield greatly decreased due to the decomposition of the free thiol on the silica gel.

2.3 Monolayer preparation and coupling reaction

According to literature [22, 29], Au films on glass substrates were treated by piranha solution (3:1 mixture of concentrated sulfuric acid and 30% hydrogen peroxide) for 5 min at room temperature, subsequently rinsed with Millipore water and abs. ethanol for 1 min, and finally dried in a nitrogen stream. This cleaning procedure was not used for the Au on mica substrates, in order to avoid the likely delamination of the Au layer [30]. The pretreated substrates were immersed in AMB ethanol solution for 45 h under argon atmosphere at room temperature. To obtain an unsaturated solution with a

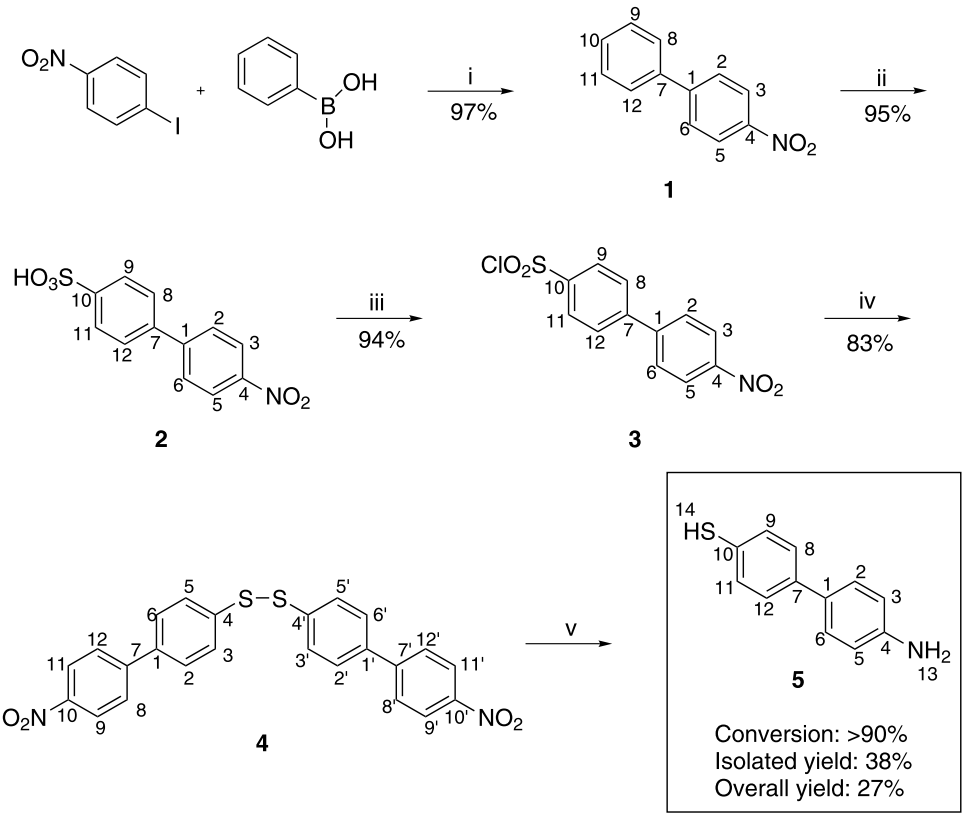

Fig. 2 Formation of 4′-amino-4-mercaptobiphenyl (AMB) via chlorosulfonation. Reagents: (i) Na_2CO_3, $Pd(OAc)_2$, H_2O, Me_2CO, 35°C, 20 min. (ii) $ClSO_3H$, dry CH_2Cl_2, 0°C, Ar, 2 h. (iii) $SOCl_2$, cat. DMF, reflux, 18 h. (iv) 1. HI (aq.), THF, 3 h; 2. $NaHSO_3$ (aq.). (v) Fe, HCl, THF, EtOH, H_2O, reflux, 3 h

reproducible concentration, AMB was placed in abs. ethanol (1 mg/40 ml) and stirred for 20 min. Then the solution was refrigerated to 4°C and filtered. The monolayers of amine were annealed at 48°C in abs. ethanol for 1 h. The sample was rinsed with abs. ethanol and dried with a nitrogen stream. For the imine bond formation [22, 31], the monolayer of amine was immediately immersed in a 10 mM solution of aldehyde in a mixture of anhydrous ethanol and trimethylorthoformate (volume ratio = 1:1) for 48 h. The sample was then rinsed with abs. ethanol and dried with nitrogen.

2.4 Contact-angle measurements

Contact angles were measured on freshly prepared samples gold-coated glass substrates with an NRL Contact-Angle Goniometer model 100-00. Millipore water was used as liquid for the drop formation. At least three drops at different locations on each sample were used.

2.5 IRRAS

Infrared reflection absorption spectra were measured using a nitrogen-purged NICOLET 8700 FT-IR spectrometer equipped with a liquid nitrogen cooled MCT detector. A molecular sieve filter device and a hydrophobic PEFT membrane made from active carbon were used to purify the nitrogen stream. All spectra were measured with a wave number resolution of 4 cm^{-1} and averaged over 2048 scans at an angle of incidence of 85° relative to the surface normal. The spectra are reported in absorbance units Log(1/R) after linear baseline correction. The spectrum of gold-coated glass washed with piranha solution for 5 min was used as reference.

2.6 XPS

X-ray photoelectron spectroscopy measurements were realized by means of a SPECS Phoibos 100 electron analyzer at a typical energy resolution of 600 meV at 20 eV pass energy. An Mg K_α X-ray tube as well as the PM-3 beamline at BESSY have been used as light sources. The excitation energies were 1253.6 and 260 eV, with photon energy resolutions of 800 and 200 meV, respectively. The binding energies have been calibrated to the Au $4f_{7/2}$ binding energy at 84.0 eV. The electron take-off angle was set to 0°, corresponding to normal emission.

2.7 NEXAFS

X-ray absorption spectra were taken using synchrotron radiation from the PM-3 dipole beamline at BESSY in Berlin, set to provide linearly polarized light with a polarization degree ≥90%. The incidence angle was varied between 20°

Table 1 Results of surface contact-angle measurements before imine formation, after the coupling reaction, and after imine hydrolysis

	Terminated functional groups	Averaged contact angle
Before imine formation	$-NH_2$	41.8°
After coupling reaction	$-CH_3$	56.6°
	$-CF_3$	55.8°
	-OH	48.2°
	-COOH	38.5°
After imine hydrolysis	$-NH_2$	42.9°

and 90° with respect to the surface plane. Absorption spectra were acquired at room temperature in total electron yield mode, recording the sample drain current as a function of photon energy. To reduce the effects of radiation damage, the photon flux density was reduced by one order of magnitude by decreasing the transmission of the beamline monochromator. Furthermore, the measuring position was moved 500 mm out of the beam focus position to reduce the photon flux density on the sample to an estimated typical flux density of about 10^{13} photons s^{-1} cm^{-2}. The energy resolution was 100 and 150 meV for the C and N *K* absorption edges, respectively.

3 Results and discussion

3.1 Preparation of the organic thin films

For the formation of self-assembled monolayers of aromatic thiols, several approaches have been published. In our case, among different solvents (dichloromethane, tetrahydrofuran, toluene, and ethanol), ethanol turned out to be the best solvent for monolayer formation, although the solubility of AMB in ethanol is quite poor. In order to obtain an unsaturated solution with a reproducible concentration, the AMB solution in ethanol was prepared by the procedure introduced in Sect. 2.3. Gold grafting was achieved with this filtrate, and the whole process was conducted under argon atmosphere to prevent the oxidation of thiol. To remove the unbonded AMB molecules from the surface, the sample was annealed by heating at 48°C in abs. ethanol for 1 h and rinsed with abs. ethanol. Before the following measurements, the samples were stored in argon atmosphere.

Contact-angle measurements can qualitatively reflect surface wetting, which relates to the hydrophilic properties of the end groups of SAMs. We detected a contact angle for bare gold of 65.5°, which decreased to 41.8° after the grafting of AMB (Table 1). In the previous studies for 4,4′-dimercaptobiphenyl [16] and 4-mercaptobiphenyl [32], the

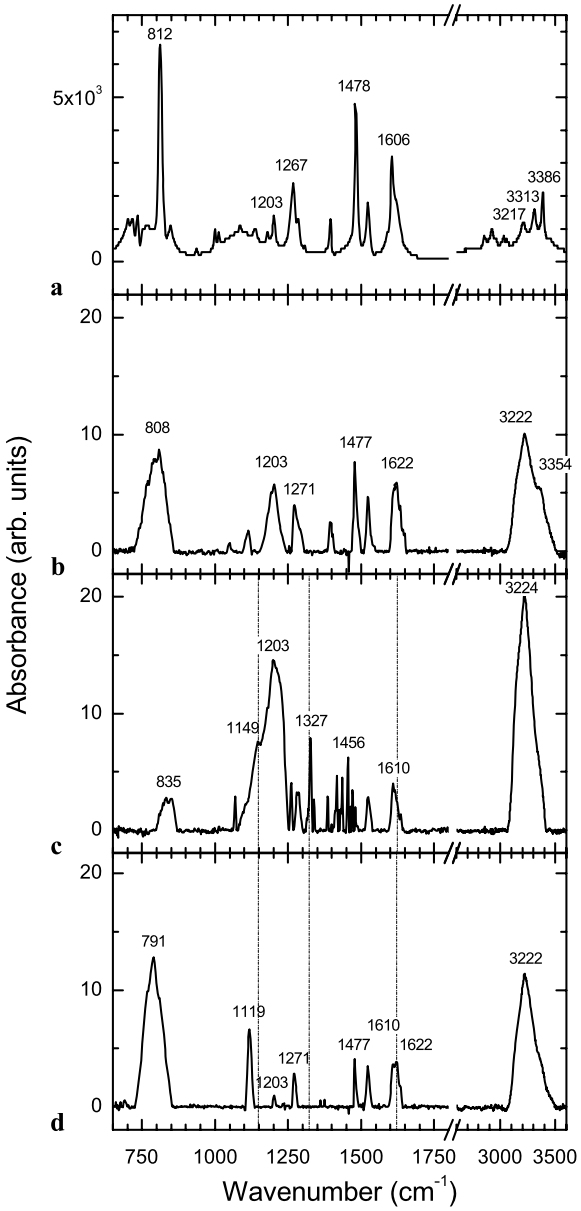

Fig. 3 IR spectra of bulk AMB in a KBr pellet (**a**), layers of AMB on gold (**b**), after imine formation (**c**), and after hydrolysis of the imine bonds (**d**)

observed contact angles were 67° and 80°, respectively. This shows that in our case amino groups ($-NH_2$), rather than thiol groups (-SH) or phenyl rings ($-C_6H_5$), should be on the top of the surface, which results in a more hydrophilic character of the surface.

In order to obtain more information about the layer assembly, IRRAS measurements were performed. Figure 3 shows that the spectra of AMB in a KBr pellet (panel (a)) and as a layer on gold (b) are comparable. We observe not only the in-plane band at 1477 cm^{-1} (Table 2), related to a transition dipole moment (TDM) oriented parallel to the ring plane and the molecular axis of the biphenyl unit, but

Table 2 Assignment of the vibrational modes probed by IRRAS in units of cm^{-1}. The abbreviations "ip" and "op" indicate in-plane and out-of-plane, respectively

	$\beta(NH_2)$	γ(C=C) ring ip	δ(CH) ring op	$\nu_s(CF_3)$	$\gamma_{as}(CF_3)$
AMB in KBr pellet	1606	1478	812	–	–
AMB on gold	1622	1477	808	–	–
After imine formation	1610	1456	835	1327	1149

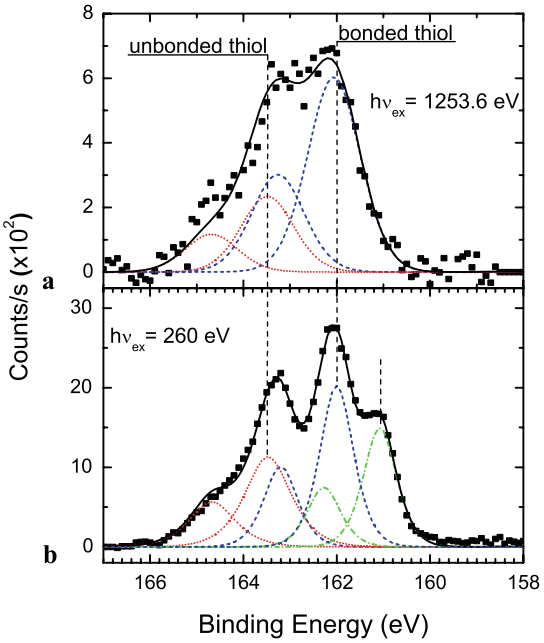

Fig. 4 S $2p$ XPS spectra for AMB adsorbed onto Au on (**a**) glass and (**b**) mica substrates. *Solid lines* represent the best fits to the experimental data (*symbols*) using two and three S $2p$ doublets for the glass and mica substrate, respectively. The S $2p_{3/2}$ peak positions are indicated by *vertical dashed lines*

also the out-of-plane band at about 810 cm^{-1} corresponding to modes with a TDM oriented perpendicularly to the ring plane of the biphenyl unit. Considering the selection rules of IRRAS spectroscopy [12, 17], these results reveal that the AMB layers are not perfectly upright on the gold surface.

XPS measurements were used to investigate the efficiency of the S–Au bond formation on glass and on mica substrates using an X-ray tube and the PM-3 beamline as light sources, respectively. Figure 4 shows the corresponding S $2p$ spectra of AMB adsorbed onto Au(111) on glass (a) and on mica (b) substrates. Both curves have been fitted with a number of peaks related to S $2p$ doublets, each

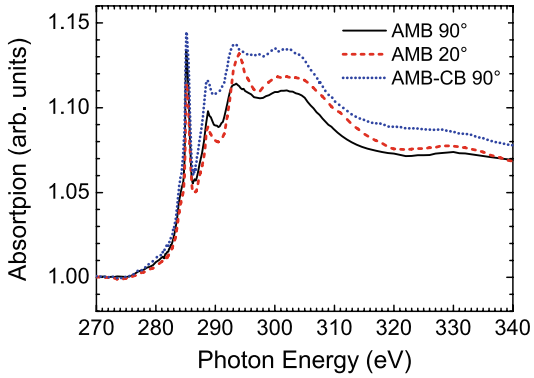

Fig. 5 C K edge NEXAFS spectra of AMB adsorbed onto Au on mica measured at normal and grazing incidence (*solid and dashed lines*). The *dotted line* shows the C K edge NEXAFS intensity of AMB-CB measured at normal incidence

of them with an area ratio of 2:1 and energy splitting of 1.2 eV. The peak line profile was chosen as the product of a Lorentzian function and a Gaussian one. In the case of the glass substrate, four peaks related to two doublets (with binding energies for the lager peaks $E_B(2p_{3/2}) = 162.0$ and 163.5 eV) can be seen [dashed and dotted lines in panel (a)]. They originate from the two chemically different species of bonded and unbonded S atoms. The peak areas of the bonded species ($E_B = 162.0$ eV) make up for 72% of the total integrated area. In the mica substrate case (panel b), an additional third doublet is identified at $E_B = 161.1$ eV (dashed–dotted line). Being at lower binding energies than the doublet corresponding to the bonded S, these shifted peaks may be caused by either S–Au bonds with different coordination numbers, as suggested in [33], or by chemical contamination of the Au layer on the mica substrate prior to the preparation of the AMB layer. In the first scenario, the total integrated area of the peaks corresponding to the bonded species yields a bonding efficiency of 73%. In the second one, i.e., neglecting the contribution of atomic S, the bonding efficiency results as 64%. In any case, we conclude that the bonding efficiency of thiolates to Au is only slightly dependent on the underlying substrate, being it glass or mica.

In order to investigate the properties of the monolayer formation of AMB molecules adsorbed on the Au layer, we performed NEXAFS experiments. Figure 5 shows the C K edge spectra of AMB and AMB-CB at different incidence angles. They consist of a series of π^* resonances at photon energies between 280 and 290 eV, and the broader σ^* resonances at photon energies above 290 eV. The two C K NEXAFS spectra of AMB taken under angles of 90° and 20° between propagation vector of the light and the surface plane show a much smaller angular dependence compared to NEXAFS measurements on a completely formed SAM [34]. The relatively small angular dependence of the π^* and σ^* resonant features can be explained by taking into account

that a fraction of AMB molecules are not bonded to the Au layer, as shown by the XPS data. The film homogeneity was confirmed by scanning the incoming X-ray beam over the sample surface.

3.2 Formation of aromatic imine-bonds on Au(111)

The carbonyl groups of different aldehydes were linked to the amino-terminated aromatic monolayers in the presence of anhydrous ethanol and trimethylorthoformate (volume ratio = 1:1) to construct in-situ a conjugated layer on the gold surface. Trimethylorthoformate was used as a dehydrating agent to accelerate the coupling reaction. Additionally, it was confirmed that anhydrous ethanol was the most effective solvent compared to dichloromethane, toluene, and tetrahydrofuran. In order to study the imine formation on the gold surface in detail, contact-angle, IRRAS, and NEXAFS measurements were carried out. 4-hydroxybenzaldehyde (HB), 4-carboxybenzaldehyde (CB), 4-methylbenzaldehyde (MB), or 4-(trifluoromethyl)benzaldehyde (TMB) were chosen as different derivatives, with either hydrophilic (-OH, -COOH) or hydrophobic groups (-CH_3, -CF_3). In principle, the surface wetting should change after imine bond formation due to the introduction of differently terminated aldehyde moieties. We observe that the improving hydrophilic performances of the end groups from methyl to carboxylic acid (hydrophilic capacity: -CH_3 ≈ -CF_3 ≪ -OH < -COOH) result in a monotonic decrease of the surface contact angle and agree with those of the terminal groups (see Table 1). These results suggest that the end groups play the major role in the alteration of the surface properties. Therefore it can be concluded that imine bonds are indeed formed. However, compared to the results of Ulman et al. using functional biphenyls [10], the surfaces in our case did not show strong hydrophobic or hydrophilic properties. Two reasons could be presumed: (i) The AMB films formed in the first step are disordered, so that the rest groups are not fully upright on the surface, and water can not access the rest groups directly; (ii) the conversion of the coupling reaction is not complete, some free amino groups still remain at the top of the layer after flushing the sample with ethanol, as indicated by surface IR and NEXAFS data.

Among these four aldehydes, 4-(trifluoromethyl)benzaldehyde was the only one chosen for IRRAS measurements, because the C–F stretching has an intense absorption in the range of 1000–1400 cm^{-1}. Two additional bands at 1327 and 1149 cm^{-1} were observed after the coupling reaction [Fig. 3(c)], which are associated to $\nu_s(CF_3)$ and $\nu_{as}(CF_3)$, respectively. Furthermore, the band of NH_2 in-plane deformation at 1622 cm^{-1} decreased significantly. This suggests that the coupling reaction worked, but only part of the amino groups converted to C=N bonds. In order to investigate this

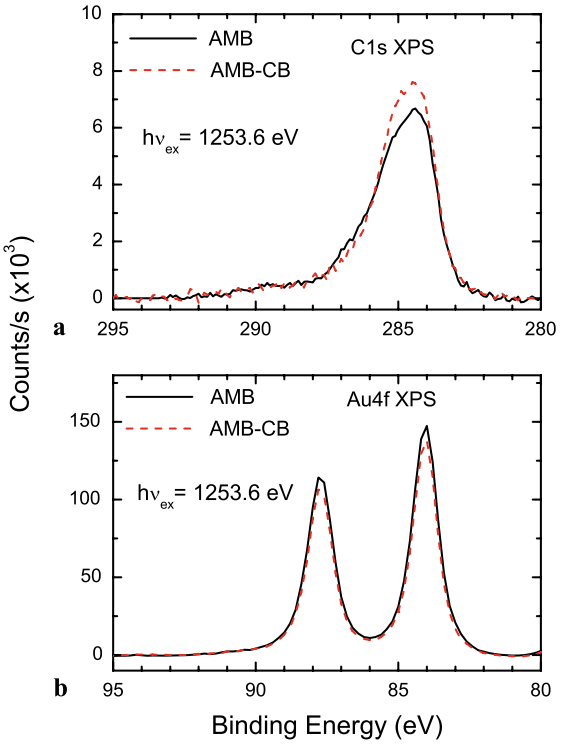

Fig. 6 (**a**) C 1*s* and (**b**) Au 4*f* XPS spectra for AMB (*full line*) and AMB-CB (*dashed*), both on glass substrates

point, the Au surface with aromatic imine bonds was immersed into Millipore water (pH ∼ 5.0) at ambient conditions for one day, and then IRRAS measurements were performed again. Hydrolysis of imine leads to the cleavage of the imine bonds to form biphenyl amine bonded to Au(111) and free aldehyde, which can be washed away with abs. ethanol. This is confirmed by the disappearance of the ν_s(CF3) and $\nu_{as}(CF_3)$ bands, while the NH_2 in-plane deformation band came back (see Fig. 3d). Moreover, the surface contact angle returned to 42.9°, which is close to the contact angle before imine formation.

Figure 6 shows the C 1*s* (panel a) and Au 4*f* (b) XPS spectra measured on the AMB and AMB-CB layers. Asymmetric Gaussian functions were employed to fit the C 1*s* peaks. The layer thicknesses before and after the imine-bond formation can be roughly estimated by comparing the relative intensities of C 1*s* and Au 4*f* XPS measurements and using terphenylthiol (TPT) on Au as a reference [12]. We used literature values for $\lambda_C = 2.9$ nm and $\lambda_{Au} = 3.5$ nm as attenuation lengths corresponding to the excitation energy of 1253.6 eV [35] and applied (1) of [12]. This yields thicknesses of 2.15 nm for the AMB and 2.3 nm for the AMB-CB layers. Compared to the expected length of an upright molecular layer of 1.0 nm this thickness estimate seems rather high. However, considering that by using the same calculation the thickness of an ordered TPT SAM was overestimated by about 40% [12], we conclude that the thickness

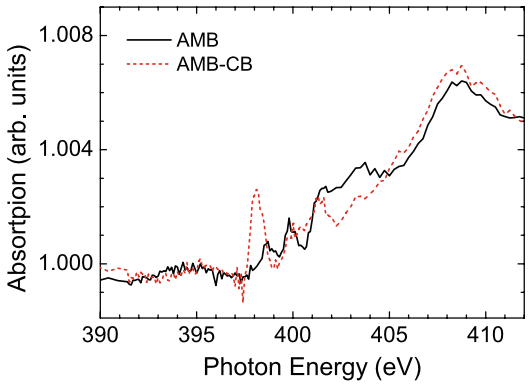

Fig. 7 N *K* edge NEXAFS spectra of AMB (*solid line*) and AMB-CB (*dashed line*) adsorbed onto Au on mica, measured at grazing incidence (20° between the light **E** vector and the surface normal)

of our AMB layer is somewhere in the range between one and two monolayers. This could well be due to the presence of unbonded molecules supported by the signal of unbonded S seen in the S 2*p* XPS data. Within the limitations of this analysis, we thus exclude the formation of thicker AMB layers. Furthermore, the moderate thickness increase of the AMB-CB layer with respect to the AMB indicates only incomplete imine bond formation.

Further information about the imine bond formation in the final AMB-CB layer comes from C and N *K* edge NEXAFS spectra. The C *K* edge spectrum of AMB-CB (dotted line in Fig. 5) shows an increase in the overall intensity by ∼13% compared to the spectrum of AMB under the same angle of incidence (solid line). This is about one third of the increase expected for a fully efficient imine bond formation.

Figure 7 shows the N *K* edge NEXAFS spectra of the AMB and AMB-CB layers on Au. The relatively low signal-to-noise ratio as compared to the C *K* edge signals is explained by the extremely low effective N concentration. The main difference between the two N *K* edge spectra is an extra π^* peak at $E = 398.1$ eV. This peak is a signature of the replacement of the two N–H σ bonds present in the amino AMB end group by the N=C double (σ and π) bond that gives rise to the final AMB-CB molecule. It can be used to estimate the N=C areal density using as a reference 1 ML Fe porphyrin molecules on metallic substrates [36]. We obtain an average areal density of one N=C bond *per* 80 Å^2. This value is smaller than the expected concentration of N=C bonds in a perfect SAM of AMB molecules but consistent with the incomplete formation of the AMB-CB layer suggested previously by contact-angle and IRRAS data.

4 Conclusion

We have succeeded in the formation of in-situ imine bonds between aromatic amino-terminated biphenyl monolayers adsorbed onto Au films and benzaldehyde derivatives. The thiol bond formation producing the AMB layer was characterized by means of IRRAS and XPS measurements, yielding about 70% bond formation efficiency. The imine bond formation of the second fabrication step has been shown by contact-angle, IRRAS, and NEXAFS data. Even though the imine-bond formation is incomplete, these results demonstrate the feasibility of this highly flexible in-situ approach for the generation of conjugated aromatic systems, with potential applications in molecular electronics and conformational switching of these functionalized surfaces.

Acknowledgements T. Kachel is acknowledged for his support during the synchrotron measurements. This work is supported by the DFG (Sfb 658).

Appendix: Synthesis of 4′-amino-4-mercaptobiphenyl

(1) *Synthesis of 4-nitrobiphenyl*

A mixture of Na_2CO_3 (212.0 mg, 2.0 mmol), $Pd(OAc)_2$ (1.1 mg, 0.005 mmol, 0.5 mol%), 1-Iodo-4-nitrobenzene (251.5 mg, 1.0 mmol, 99%), phenylboronic acid (186.6 mg, 1.5 mmol, 98%, 1.5 eq.), distilled water (3.5 ml), and p.a. acetone (3 ml) was stirred for 20–30 min at 35°C. The reaction solution was extracted three times with diethyl ether. The combined organic phase was washed with brine and dried over $MgSO_4$. The further purification of the product was achieved by chromatography on silica gel column (Hexane:Ethylacetate = 5:1), giving a light yellow crystalline solid (194.1 mg) with the yield of 97%.

IR (KBr): ν (cm^{-1}) = 1513.89 (NO_2 asymmetric stretching), 1344.86 (NO_2 symmetric stretching), 853.65 (1,4-disubstituted, CH wagging), 740.78 (mono-substituted, CH-wagging);

1H NMR (500 MHz, $CDCl_3$): δ (ppm) = 8.30 (d, 2H, 3,5-H), 7.74 (d, 2H, 2,6-H), 7.63 (d, 2H, 8,12-H), 7.51 (t, 2H, 9,11-H), 7.45 (t, 1H, 10-H);

^{13}C NMR (125 MHz, $CDCl_3$): δ (ppm) = 147.59 (1-C), 147.05 (4-C), 138.73 (7-C), 129.13 (9,11-C), 128.89 (10-C), 127.76 (2,6-C), 127.35 (8,12-C), 124.07 (3,5-C); MS (EI): m/z = 199.0 (100%, $[M]^+$, calcd. for $C_{12}H_9NaO_2$: 199.06).

(2) *Synthesis of 4′-nitrobiphenyl-4-sulfonic acid*

Chlorosulfonic acid (0.34 ml, 4.93 mmol) was slowly added to an ice-cooled solution of 4-nitrobiphenyl (982.4 mg, 4.93 mmol, 0.2 M) in dry CH_2Cl_2 (25 ml) under Argon atmosphere, and the mixture was stirred for 2 h at 0°C. The solvent was then evaporated and the residue washed with p.a. chloroform, then dried under vacuum, giving a white solid (1.312 g) with a yield of 95%.

^{1}H NMR (500 MHz, DMSO): δ (ppm) = 8.29 (d, 2H, 3,5-H), 7.96 (d, 2H, 9,11-H), 7.75 (m, 4H, 2,6,8,12-H);

^{13}C NMR (125 MHz, DMSO): δ (ppm) = 148.70 (10-C), 147.00 (4-C), 146.36 (1-C), 138.20 (7-C), 128.19 (8,12-C), 127.13 (2,6-C), 126.65 (9,11-C), 124.37 (3,5-C);

MS (neg. ESI-TOF): $m/z = 278.0$ ([M-H]$^-$, calcd. for $C_{12}H_8NO_5S$: 278.02).

(3) *Synthesis of 4′-nitrobiphenyl-4-sulfonyl chloride*

4′-nitrobiphenyl-4-sulfonic acid (140.7 mg, 0.5 mmol) was refluxed in thionyl chloride (2 ml) with a catalytic quantity of DMF (33.3 µl) for 18 h. Then toluene was added and the solvents were evaporated under vacuum to give a yellow crystalline solid (139.3 mg) with a yield of 94%.

^{1}H NMR (250 MHz, $CDCl_3$): δ (ppm) = 8.37 (d, 2H, 3,5-H), 8.17 (d, 2H, 9,11-H), 7.82 (m, 4H, 2,6,8,12-H);

^{13}C NMR (62.5 MHz, DMSO): δ (ppm) = 148.23 (4-C), 145.65 (7-C), 144.68 (10-C), 144.25 (1-C), 128.63, 128.43 (8,9,11,12-C), 127.81 (2,6-C), 124.41 (3,5-C);

MS (EI): $m/z = 296.9$ ([M]$^+$, calcd. for $C_{12}H_8NO_4SCl$: 296.99).

(4) *Synthesis of 1,2-bis(4′-nitrobiphenyl-4-yl)disulfane*

An aqueous solution of hydriodic acid (1.52 ml, 57 wt.%) was rapidly added to a mixture of 4′-nitrobiphenyl-4-sulfonyl chloride (297.7 mg, 1 mmol) in 3 ml p.a. THF while stirring. The reaction temperature increased and the mixture turned brown. The reaction was stirred at r.t. for 3 h, followed by addition of an aq. sodium bisulfite solution (649.6 mg in 1.5 ml distilled water). The reaction solution turned to yellow slowly. The precipitate was collected by vacuum filtration, washed with H_2O (20 ml), and dried under low pressure. The further purification of the product was achieved by flash chromatography on a silica gel column (CH_2Cl_2), giving a yellow powder (192.0 mg) with a yield of 83%.

IR (KBr): ν (cm^{-1}) = 1516.96, 1505.61 (NO_2 asymmetric stretching), 1340.15 (NO_2 symmetric stretching), 817.03 (1,4-disubstituted, CH wagging);

^{1}H NMR (500 MHz, $CDCl_3$): δ (ppm) = 8.29 (d, 4H, 9,11,9′,11′-H), 7.70 (d, 4H, 8,12,8′,12′-H), 7.65 (d, 4H, 3,5,3′,5′-H), 7.58 (d, 4H, 2,6,2′,6′-H);

^{13}C NMR (62.5 MHz, DMSO): δ (ppm) = 147.30 (10,10′-C), 146.44 (7,7′-C), 137.96 (4,4′-C), 137.79 (1,1′-C), 128.06 (3,3′,5,5′-C), 127.95 (8,8′,12,12′-C), 127.58 (2,2′,6,6′-C), 124.20 (9,9′,11,11′-C);

MS (EI): $m/z = 460.05$ ([M]$^+$, calcd. for $C_{24}H_{16}N_2O_4S_2$: 460.06).

(5) *Synthesis of 4′-amino-4-mercaptobiphenyl*

1,2-bis(4′-nitrobiphenyl-4-yl)disulfane (230.3 mg, 0.5 mmol), 1.96 ml p.a. ethanol, 1.53 ml distilled water, and 13 ml p.a. THF were placed in a 50 ml, three-necked flask, fitted with a reflux condenser and a mechanical stirrer. More p.a. THF can be added if necessary to ensure that all starting material completely dissolves in the mixed solvent at 60°C. Then, iron powder (171.2 mg, 6.1 eq.) was added, and the mixture was stirred followed by the addition of conc. HCl (10 µl). The resultant mixture was heated to 80°C for 3 h. It was then vacuum filtered, while hot and the filtrate was evaporated under reduced pressure. The residue was successively dissolved in CH_2Cl_2 and washed with water and brine, then dried under vacuum. The further purification was achieved by chromatography on a silica gel column (CH_2Cl_2), giving a yellow powder (76.3 mg) with a yield of 38%.

IR (KBr): ν (cm^{-1}) = 3386.39 (NH_2 asymmetric stretching), 3313.11 (NH_2 symmetric stretching), 1606.41 (NH_2 in plane deformation), 811.88 (1,4-disubstituted, CH wagging);

^{1}H NMR (400 MHz, CD_2Cl_2, a drop of DMSO-d_6): δ (ppm) = 7.50 (dd, 4H, 2,6,8,12-H), 7.36 (d, 2H, 9,11-H), 6.70 (d, 2H, 3,5-H), 4.01 (br, 2H, 13-H), 2.30 (br, 1H, 14-H);

^{13}C NMR (100 MHz, CD_2Cl_2, a drop of DMSO-d_6): δ (ppm) = 147.66 (1-C), 140.80 (4-C), 134.36 (7-C), 128.96 (9,11-C), 128.88 (10-C), 127.70 (2,6-C), 126.75 (8,12-C), 115.05 (3,5-C);

MS (EI): $m/z = 201.0$ ([M]$^+$, calcd. for $C_{12}H_{11}NS$: 201.06).

References

1. F. Schreiber, Prog. Surf. Sci. **65**, 151–256 (2000)
2. J.C. Love, L.A. Estroff, J.K. Kriebel, R.G. Nuzzo, G.M. Whitesides, Chem. Rev. **105**, 1103–1170 (2005)
3. M.J. Mackel, S. Sanchez, J.A. Kornfield, Langmuir **23**, 3–7 (2007)
4. R. Yamada, H. Tada, Langmuir **21**, 4254–4256 (2005)
5. J. Scherer, M.R. Vogt, O.M. Magnussen, R.J. Behm, Langmuir **13**, 7045–7051 (1997)
6. J.D. Patel, M. Ebert, K. Stokes, R. Ward, J.M. Anderson, J. Biomater. Sci. Polym. Edn. **14**, 279–295 (2003)
7. K.L. Prime, G.M. Whitesides, Science **252**, 1164–1167 (1991)
8. B. de Boer, H. Meng, D.F. Perepichka, J. Zheng, M.M. Frank, Y.J. Chabal, Z. Bao, Langmuir **19**, 4272–4284 (2003)
9. J. Kang, A. Ulman, R. Jordan, D. Kurth, Langmuir **15**, 5555–5559 (1999)
10. J.F. Kang, S. Liao, R. Jordan, A. Ulman, J. Am. Chem. Soc. **120**, 9662–9667 (1998)
11. H.-J. Himmel, A. Terfort, C. Wöll, J. Am. Chem. Soc. **120**, 12069–12074 (1998)
12. C. Fuxen, W. Azzam, R. Arnold, G. Witte, A. Terfort, C. Wöll, Langmuir **17**, 3689–3695 (2001)
13. W. Azzam, B.I. Wehner, R.A. Fischer, A. Terfort, C. Wöll, Langmuir **18**, 7766–7769 (2002)
14. J. Kang, R. Jordan, A. Ulman, Langmuir **14**, 3983–3985 (1998)
15. J.F. Kang, A. Ulman, S. Liao, R. Jordan, Langmuir **15**, 2095–2098 (1999)
16. J.F. Kang, A. Ulman, S. Liao, R. Jordan, G. Yang, G.-Y. Liu, Langmuir **17**, 95–106 (2001)
17. Y. Tai, A. Shaporenko, H.-T. Rong, M. Buck, W. Eck, M. Grunze, M. Zharnikov, J. Phys. Chem. B **108**, 16806–16810 (2004)
18. A. Shaporenko, K. Heister, A. Ulman, M. Grunze, M. Zharnikov, J. Phys. Chem. B **109**, 4096–4103 (2005)
19. G. Heimel, L. Romaner, J.-L. Brédas, E. Zojer, Phys. Rev. Lett. **96**, 196806 (2006)
20. M.B. Smith, J. March, *March's Advanced Organic Chemistry: Reactions, Mechanisms, Structure, Sixth Edition* (Wiley, New York, 2007)
21. J.J.W.M. Rosink, M.A. Blauw, L.J. Geerligs, E. van der Drift, B.A.C. Rousseeuw, S. Radelaar, W.G. Sloof, E.J.M. Fakkeldij, Langmuir **16**, 4547–4553 (2000)

22. J.E. Klare, G.S. Tulevski, C. Nuckolls, Langmuir **20**, 10068–10072 (2004)
23. J.M. Tour, Chem. Rev. **96**, 537–554 (1996)
24. N.C. Gianneschi, P.A. Bertin, S.T. Nguyen, C.A. Mirkin, L.N. Zakharov, A.L. Rheingold, J. Am. Chem. Soc. **125**, 10508–10509 (2003)
25. L. Liu, Y. Zhang, B. Xin, J. Org. Chem. **71**, 3994–3997 (2006)
26. M.A. Santos, S.M. Marques, T. Tuccinardi, P. Carelli, L. Panelli, A. Rossello, Prog. Surf. Sci. **14**, 7539–7550 (2006)
27. I.R. Greig, A.I. Idris, S.H. Ralston, R.J. van'tHof, J. Med. Chem. **49**, 7487–7492 (2006)
28. M. Zhang, D. Ryckman, G. Chen, E. MacMillan, J. Duquette, Synthesis (2003) 112–116
29. R. Arnold, A. Terfort, C. Wöll, Langmuir **17**, 4980–4989 (2001)
30. J. Kang, P.A. Rowntree, Langmuir **23**, 509–516 (2007)
31. B. Ruhland, A. Bhandari, E.M. Gordon, M.A. Gallop, J. Am. Chem. Soc. **118**, 253–254 (1996)
32. Y.-T. Tao, C.-C. Wu, J.-Y. Eu, W.-L. Lin, Langmuir **13**, 4018–4023 (1997)
33. D.G. Castner, K. Hinds, D.W. Grainger, Langmuir **12**, 5083–5086 (1996)
34. S. Frey, V. Stadler, K. Heister, W. Eck, M. Zharnikov, M. Grunze, B. Zeysing, A. Terfort, Langmuir **17**, 2408–2415 (2001)
35. C.D. Bain, G.M. Whitesides, J. Phys. Chem. **93**, 1670–1673 (1989)
36. H. Wende, M. Bernien, J. Luo, C. Sorg, N. Ponpandian, J. Kurde, J. Miguel, M. Piantek, X. Xu, Ph. Eckhold, W. Kuch, K. Baberschke, P.M. Panchmatia, B. Sanyal, P.M. Oppeneer, O. Eriksson, Nat. Mater. **6**, 516–520 (2007)